Available online at www.sciencedirect.com
SCIENCE DIRECT®
Journal of Inorganic Biochemistry 98 (2004) 1686–1695
JOURNAL OF Inorganic Biochemistry
www.elsevier.com/locate/jinorgbio

Crystal structures of ferrous and ferrous–NO forms of verdoheme in a complex with human heme oxygenase-1: catalytic implications for heme cleavage

Latesh Lad [a,b,c], Paul R. Ortiz de Montellano [d], Thomas L. Poulos [a,b,c,*]

[a] *Department of Molecular Biology and Biochemistry, University of California, 2206 Natural Sciences 1, Irvine, CA 92697-3900, USA*
[b] *Department of Chemistry, University of California, 2206 Natural Sciences 1, Irvine, CA 92697-3900, USA*
[c] *Department of Physiology and Biophysics, and Program in Macromolecular Structure, University of California, 2206 Natural Sciences 1, Irvine, CA 92697-3900, USA*
[d] *Department of Pharmaceutical Sciences, School of Pharmacy, University of California, San Francisco, CA 94143-0446, USA*

Received 2 June 2004; received in revised form 7 July 2004; accepted 8 July 2004
Available online 28 August 2004

Abstract

Heme oxygenase oxidatively degrades heme to biliverdin resulting in the release of iron and CO through a process in which the heme participates both as a cofactor and substrate. One of the least understood steps in the heme degradation pathway is the conversion of verdoheme to biliverdin. In order to obtain a better understanding of this step we report the crystal structures of ferrous–verdoheme and, as a mimic for the oxy–verdoheme complex, ferrous–NO verdoheme in a complex with human HO-1 at 2.20 and 2.10 Å, respectively. In both structures the verdoheme occupies the same binding location as heme in heme–HO-1, but rather than being ruffled verdoheme in both sets of structures is flat. Both structures are similar to their heme counterparts except for the distal helix and heme pocket solvent structure. In the ferrous–verdoheme structure the distal helix moves closer to the verdoheme, thus tightening the active site. NO binds to verdoheme in a similar bent conformation to that found in heme–HO-1. The bend angle in the verodoheme–NO structure places the terminal NO oxygen 1 Å closer to the α-*meso* oxygen of verdoheme compared to the α-*meso* carbon on the heme–NO structure. A network of water molecules, which provide the required protons to activate the iron–oxy complex of heme–HO-1, is absent in both ferrous–verdoheme and the verdoheme–NO structure.

Keywords: Heme oxygenase; Verdoheme; Mechanism; Crystallography

1. Introduction

Heme oxygenase (HO) catalyzes the NADPH, O_2 and cytochrome P450 reductase dependent oxygenation of heme to iron, biliverdin and carbon monoxide [1] (Fig. 1). Mammalian HO exists as two isoforms, HO-1 and HO-2, with essentially identical enzyme activities. Inducible HO-1 is primarily involved in heme catabolism in the liver and spleen while the constitutive HO-2 may serve as a source of CO, a putative messenger molecule in various physiological functions [2–4]. The basic HO-1 catalyzed oxidation of heme involves rapid hydroxylation at the α-*meso* carbon of the heme, oxygen-dependent fragmentation of α-*meso*-hydroxyheme to verdoheme, and oxidative cleavage of verdoheme to biliverdin [5]. The first electron provided by the P450 reductase reduces the ferric heme iron to the ferrous state, and a molecule of oxygen binds to form a metastable O_2-bound complex which is reduced by a second electron to generate ferric–hydroperoxy HO (Fe(III)–OOH) [6]. According to detailed

* Corresponding author. Tel.: +1 949 824 7020; fax: +1 949 824 3268.
E-mail address: poulos@uci.edu (T.L. Poulos).

0162-0134/$ - see front matter © 2004 Elsevier Inc. All rights reserved.
doi:10.1016/j.jinorgbio.2004.07.004

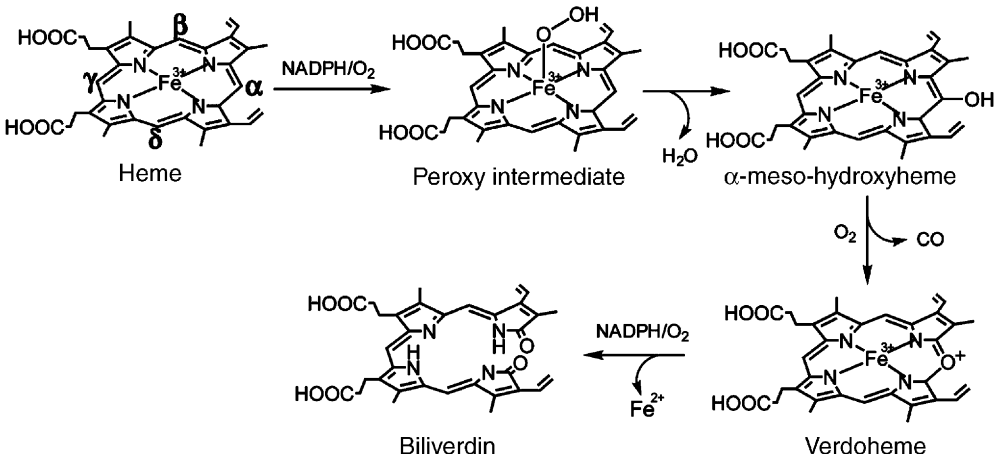

Fig. 1. The overall reaction catalyzed by heme oxygenase that results in the oxidation of heme and release of the α-*meso* carbon atom as CO.

spectroscopic studies [7], the next step is electrophilic addition of the reactive Fe(III)–OOH species to the heme α-*meso* carbon. This is in contrast to peroxidases and cytochrome P450 that proceed through a high-valent ferryl (Fe(IV)–O) active intermediate [8] as the reactive hydroxylating species rather than a peroxo ligand capable of attacking the a-*meso* bridge of the heme (Fig. 1). The exact stoichiometric requirements involved in the formation of ferric verdoheme from a-*meso*-hydroxyheme have been controversial [9] although there is general agreement that this process is oxygen-dependent.

Both rat and human isoforms of HO-1 contain C-terminal hydrophobic sequences that provide anchors to the microsomal membrane. However, the expression of soluble, truncated forms of HO-1 that lack the membrane-binding domain while retaining activity [10] greatly facilitated detailed mechanistic studies of these enzymes. Most notable were the crystallization and structure determination of human and rat HO-1 enzymes complexed with heme [11,12], which provided significant insights into both the mechanism and regiospecificity of the HO reaction. The crystal structure of human HO-1 in a complex with heme revealed a novel protein fold that consists primarily of α-helices with the heme sandwiched between the proximal and distal helices [12]. In the human HO-1 structure conserved glycines in the distal pocket provide flexibility that allows the two molecules in the crystallographic asymmetric unit cell to differ. In one molecule the active site pocket is more open with a relatively loose distal helix-heme contact, while in the other molecule the contact between the heme and distal helix is tighter. This, together with the high crystallographic thermal factors, suggest that flexibility of the distal helix enables the heme pocket to be opened and closed to bind the heme substrate and to permit dissociation of the biliverdin product.

Significant advances have been made in understanding HO structure function through a combination of protein engineering [13–16], X-ray crystallography [11,12,17–25], and NMR spectroscopy [26–31]. To briefly summarize, flexibility in the heme pocket, especially the distal helix, helps to trap important water molecules in the active site that form a conserved H-bonded network with key amino side chains such as Asp140 in HO-1. The purpose of this network is to deliver a proton to the iron-linked dioxygen required for catalysis. This H-bonded network together with steric factors orient dioxygen or peroxide toward the α-*meso* heme carbon for regioselective electrophilic attack by the distal peroxide OH group. The crystal structure of α-*meso*-hydroxyheme has not yet been solved but various spectroscopic approaches have advanced our understanding of the conversion of hydroxy-heme to verdoheme [9,32–35]. The recent crystal structures of the biliverdin-iron chelate rat HO-1 complex [22] and the biliverdin human HO-1 complex [25] have a provided structural insights in the final step in the heme degradation pathway.

The conversion of verdoheme to biliverdin is the least well-characterized step of the overall reaction. The conversion of verdoheme to biliverdin requires reducing equivalents and oxygen [36–38] and both lactam oxygen atoms in biliverdin derive from O_2 [39,40]. A mechanism has been proposed [41] which involves the binding of dioxygen to the Fe^{2+} verdoheme, dioxygen bond cleavage through either an alkoxy anion or radical, ring cleavage, and a two-electron reduction to produce ferric biliverdin. To help clarify this step of the HO reaction, we have solved the crystal structure of ferrous–verdoheme and, as a mimic for the oxy–verdoheme complex, ferrous–NO form of verdoheme in a complex with human HO-1 at 2.20 and 2.10 Å, respectively.

2. Materials and methods

2.1. Materials

Verdoheme (Fe^{2+}) was custom synthesized from biliverdin by Frontier Scientific Inc. (Utah, USA) accord-

ing to previously reported procedures [42]. The truncated water-soluble form of recombinant human HO-1 was expressed, purified, and reconstituted with hemin according to published procedures [10,15,43].

2.2. Formation and crystallization of verdoheme–HO-1 complex

For the preparation of the verdoheme–HO-1 complex, apo human HO-1 solution in CO-saturated 0.1 M potassium phosphate buffer (pH 7.4) was carefully mixed with the verdoheme dissolved in a mixture (5% v/v) of pyridine and CO-saturated 0.1 M potassium phosphate buffer (pH 7.4). Excess verdoheme was removed by passing the complex down a Sephadex G25 column equilibrated with CO-saturated potassium phosphate (pH 7.4). Formation and authenticity of the complex was confirmed by UV/Vis absorption spectroscopy, using the spectral data from Balch et al. as the standard [44].

The verdoheme–HO-1 complex crystals were grown differently than those of the heme–HO-1 crystals. During crystal screening it was found that in the absence of CO the verdoheme would degrade, and as result it was necessary to crystallize the CO–verdoheme complex by the following procedure. A solution consisting of 2.0 M ammonium sulphate, 0.1 M Hepes, pH 8.0 and 200 mM KCl were first made anaerobic by repeated exchange with O_2-free argon and nitrogen on a vacuum mainifold and then saturated with CO. Capillaries for crystal growth were quartz and 2.0 mm in diameter that were pre-sealed at one end (Hampton Scientific). Capillaries were set up and crystal growth was carried out in a custom made anaerobic chamber, which could be continuously purged with CO via an air tight outlet valve. The CO saturated precipitant solution (100 μl) was placed at the bottom of the capillary and 80 μl of the CO saturated protein solution (30 mg ml^{-1}) was layered on top. Capillaries were quickly purged with CO before being sealed with epoxy and stick wax (Hampton Scientific). The capillaries were placed in the anaerobic box, which was continuously purged with CO until crystals of the verdoheme–HO-1 were obtained. For cryogenic data collection D-(+)-trehalose was used as the cryoprotectant. Cryogenic data collection involved a three step transfer to anaerobic artificial precipitant solution, pre-saturated with CO, with increased D-(+)-trehalose concentration up to 35% (v/v) D-(+)-trehalose in a soft-sided glove box (Coy, Grass Lake, Michigan). In order to obtain a complete CO-free verdoheme–HO-1 complex, the final step of the three step cryogenic soak was done in the absence of CO, but still under strict anaerobic conditions, prior to freezing. The verdoheme–HO-1 complex crystals belong to the monoclinic space group, $P2_1$. Cell dimensions of all complexes are listed in Table 1.

Table 1
Data collection and refinement statistics

	Verdoheme	Verdoheme–NO
Crystal data		
Radiation source	Synchrotron	Synchrotron
Space group	$P2_1$	$P2_1$
Cell parameters (Å) and β (°)	61.60	61.03
	54.56	54.25
	71.72	70.25
	99.24	98.12
Data collection		
Detector distance (nm)	140	140
Molecules per asymmetric unit	2	2
Resolution (Å)	2.20	2.10
Mosaicity (°)	0.52	1.38
Total observations	1,89,098	2,99,776
Unique reflections	67,199	79,654
Completeness (%)	99.9	93.8
Mean I/σ	11.4(2.2)	10.3(2.0)
R_{sym} (%)	4.9(41.7)	5.5(25.5)
Refinement statistics		
R_{cryst}[a]	0.196	0.241
R_{free}	0.238	0.276
r.m.s.[b] *d* bond lengths (Å)	0.006	0.006
r.m.s.[b] *d* angles (°)	1.1	1.1
Water molecules	259	195
Ramachandran angles		
Most favored (%)	96.2	95.1
Additional allowed (%)	3.8	4.9

[a] $R_{cryst} = \sum(|F_{obs}| - |F_{calc}|)/\sum|F_{obs}|$. The R_{free} is the R_{cryst} calculated on the 5% reflections excluded for refinement.

[b] r.m.s. bond and r.m.s. angle represent the root-mean-squared deviation between the observed and ideal values.

2.3. Generation of the verdoheme–HO-1 NO complex

Crystals of the verdoheme–HO-1 complex were passed stepwise through the normal (as described above) three step transfer to anaerobic artificial precipitant solution pre-saturated with NO with increased D-(+)-trehalose concentration up to 35% (v/v) D-(+)-trehalose. The cryoprotectant solution and the cryo-soaked crystals were transferred into a sealed serum vial before being purged with NO gas for approximately 10 min. The crystals in the presence of NO were left to stand for a further 20 min before being flash frozen for data collection.

2.4. Data collection

Crystal screening was performed on an R-AXIS IV imaging plate detector equipped with a rotating copper anode X-ray generator with Yale focusing mirrors (Rigaku). Crystals were maintained at −160 °C in a steam of nitrogen (Crystal Logic, Los Angeles). High-resolution data collection was performed at ALS beamline 5.0.2 with a charge-coupled device (CCD). Optimi-

zation of data collection was guided by STRATEGY function of MOSFLM [45]. All data were reduced using HKL 2000 [46], and rejections were performed with ENDHKL (Louis Sanchez, California Institute of Technology) in conjunction with SCALEPACK. For all data collection, a 180° scan using 1° frames was collected.

2.5. Model building and refinement

Both the verdoheme and verdoheme–NO complex crystals were found to be isomorphous with that of the heme–HO-1 crystals [12]. As a result the structure of the heme–HO-1 complex (PDB Accession No. 1qq8) [12] was used as the starting model for refinement in CNS [47]. Rigid body refinement was followed by slow-cool simulated annealing to remove phase bias and the remaining cycles that followed consisted of a few cycles of conjugate gradient minimization and water picking. Finally, temperature factors were refined. No restraints for non-crystallographic symmetry were applied. The verdoheme was clearly present in the initial map and therefore was included in subsequent refinement. The program O [48] was used for further adjustment and modeling of protein atoms, ligands and water molecules. Backbone geometry was checked in PROCHECK [49], and none of the residues were in the disallowed region. Diffraction and refinement statistics for all structures are summarized in Table 1.

2.6. Protein data bank accession codes

PDB coordinates have been deposited in the Protein Data Bank (Accession Codes, 1TWN and 1TWR).

3. Results

3.1. Overall structure and crystallization of the verdoheme–HO-1 complex

In the presence of air the verdoheme in HO-1 degrades [34]. However, even under anaerobic conditions HO-1 reconstituted with verdoheme would degrade within 20–48 h (data not shown) which precluded crystallization of the verdoheme complex. However, the reduced-CO complex was indefinitely stable so we focused on crystallizing the HO-1–verdoheme–CO complex. To ensure that the verdoheme had not degraded during cryogenic soaking, freezing or data collection, UV/Vis absorption spectra were recorded from crystals after data collection. As shown in Fig. 2, the vedoheme–HO-1 complex spectrum remains the same before and after data collection.

The structure of the verdoheme–HO-1 complex has been refined to an R factor of 0.19 and free R factor of 0.23 at 2.20 Å resolution. There are two molecules in the asymmetric unit (labeled A and B), each with residues 10–233 resolved, along with a substrate verdoheme in each molecule. The final model contains a total of 2492 protein atoms and 260 water atoms. As with the heme–HO-1 structure we refer to the two molecules in the asymmetric unit of verdoheme–HO-1 as being open and closed. In the closed conformation, the distal helix is closer to the substrate, thus forming a tighter active-site pocket. The structure of the verdoheme–HO-1 complex is very similar to that heme–HO-1 [12], with a root-mean square deviation for the Cα atoms only being 0.19 Å. The only significant difference is between the closed molecules where there is a large deviation in the distal helix (Fig. 3).

3.2. Active site protein structure of the verdoheme–HO-1 complex

Differences between Fe(II)–verdoheme and Fe(III)–heme are very similar to the changes resulting from reduction of Fe(III)–heme to Fe(II)–heme. The largest changes are in the distal helix that runs over one face of the verdoheme. The main differences are confined to the middle of the distal helix and solvent structure in the active site. In the heme–HO-1 structure the distal helix sits over the face of the heme where ligands bind and is

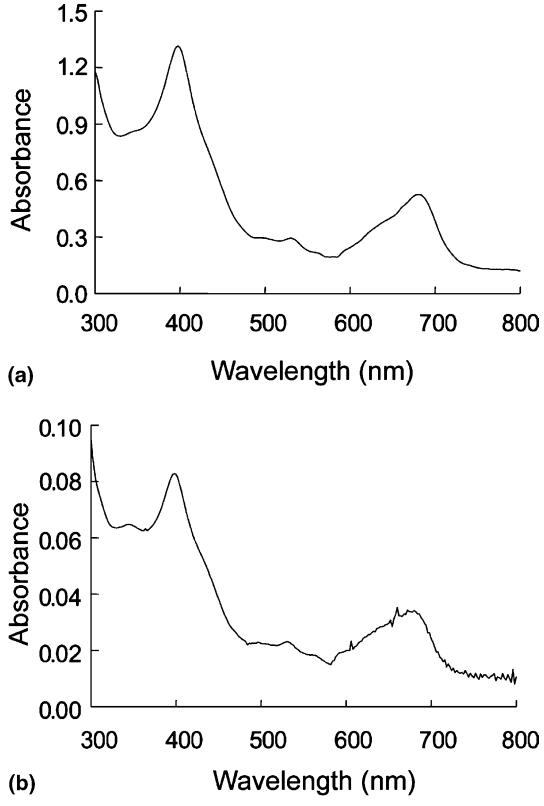

Fig. 2. UV/visible spectra of verdoheme–HO-1 (a) in solution and (b) a dissolved single crystal after data collection. All spectra were taken in anaerobic cuvettes containing oxygen free 20 mM phosphate, pH 7.5, 20 °C and 1% pyridine.

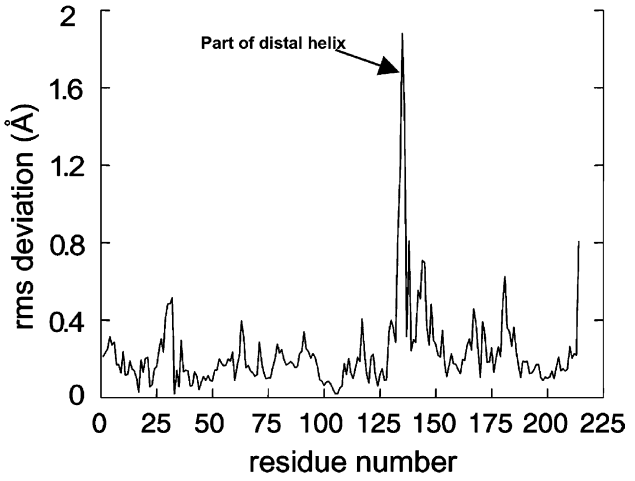

Fig. 3. Least-squares superimposition between the closed molecules of verdoheme–HO-1 and heme–HO-1.

kinked by approximately 50° directly over the heme. Based on the substrate bound (heme), substrate free (apo) and product bound (biliverdin) human HO-1 structures the stretch of conserved glycines in the distal helix (Gly139, Gly143 and Gly144) are responsible for the kink and the required flexibility to bind substrate and release product [12,18,25]. In verdoheme–HO-1 part of the distal helix (Leu141 to Lys148) that runs along one face of verdoheme moves closer to the verdoheme. This region of the distal helix includes the conserved Gly143 and Gly144, which move approximately 1.5–2.0 Å closer to verdoheme than heme in heme–HO-1 (Fig. 4). The various H-bonded distances suggest that the tightened region of the distal helix is not very stable. For instance, in heme–HO-1 the carbonyl oxygens of Gly143 and Gly144 form stabilizing H-bonds with the peptide backbones of Leu147 (3.0 Å) and Lys148 (2.9 Å), respectively, and the carbonyl oxygen of Ser142 forms a strong H-bond with the side chain of Gln145 (2.6 Å). The same set of H-bonds in verdoheme–HO-1 are stretched if not broken. For example, the H-bonding distance between Gly143 and Leu147 is 3.2 Å while that for Gly144 and Lys148 is 3.04 Å. The distance between Ser142 carbonyl oxygen and side chain of Gln145 increases to 3.75 Å owing to a repositioning of the Gln145 side chain. As noted earlier, these same changes are observed in going from Fe(III)–heme to Fe(II)–heme.

3.3. Verdoheme structure and protein interactions

Fig. 5 shows an omit electron density map for verdoheme in the closed molecule of verdoheme–HO-1. A majority of the verdoheme structure is well defined, but only one of the heme propionates is visible and the apparently disordered propionate was omitted from the model. The most noticeable difference observed when the heme of heme–HO-1 is that the verdoheme is clearly more planar (Fig. 5). Again this may have to due with the redox state of the heme iron since a very similar flattening of the heme was observed upon reduction of the heme iron from Fe(III) to Fe(II) [20]. The planar/flat conformation of verdoheme in human HO-1 is consistent with the verdoheme analogues $[(OEOP)Fe^{II}Cl_2]$ and $[(OEOP)Fe^{II}Br_2]$, where (OEP) is the dianion octaethyloxoporphyrin [44]. The average distance between the iron and pyrrole nitrogens of verdoheme in HO-1 also compare favorably with those reported for the verdoheme analogues with an average distance being 2.04 Å for the verdoheme in HO-1 compared to 2.07 to 2.09 Å for $[(OEOP)Fe^{II}Cl_2]$ and $[(OEOP)Fe^{II}Br_2]$, respectively.

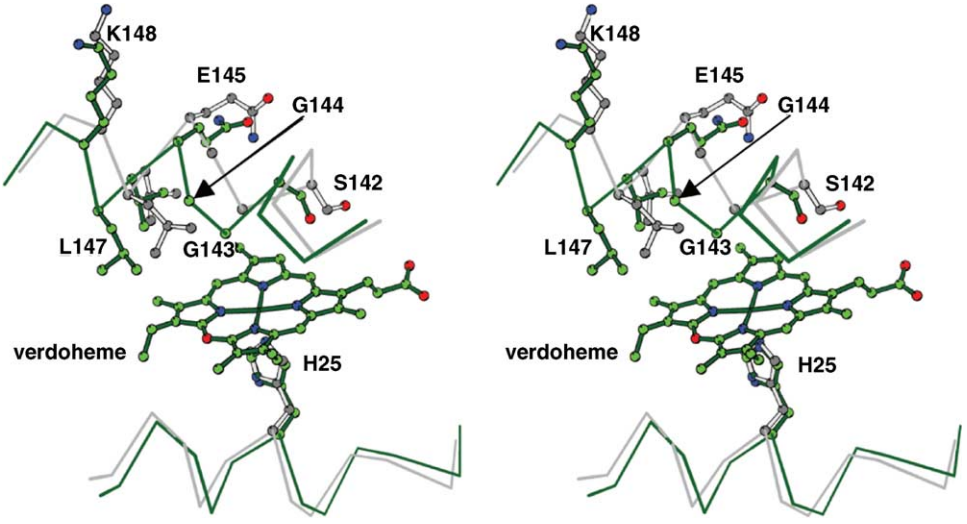

Fig. 4. Stereo diagram comparing the distal and proximal verdoheme region between the closed conformation of heme–HO-1 (grey) and verdoheme–HO-1 (green).

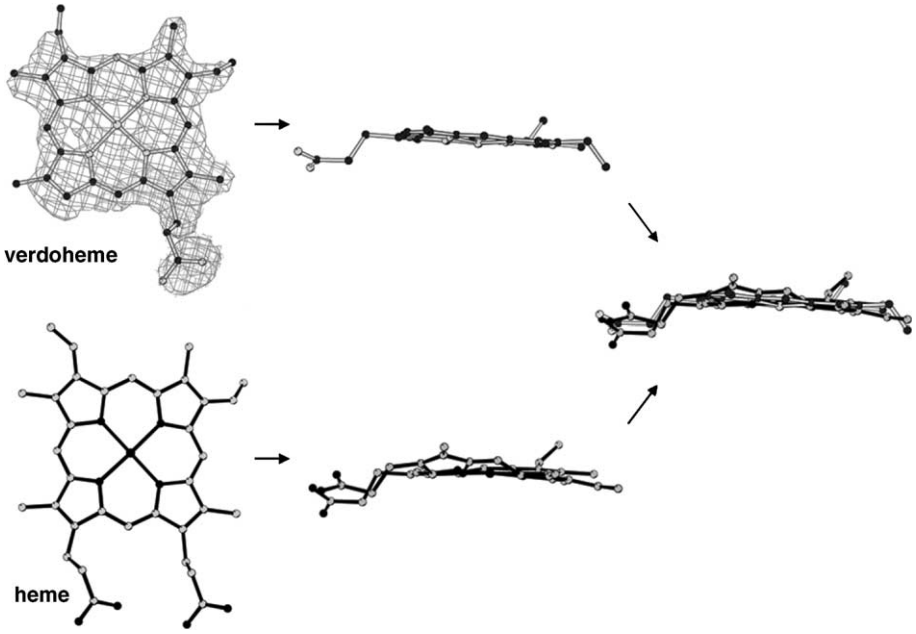

Fig. 5. Comparison of substrate structure of heme (black) and verdoheme (grey) in human HO-1. Top left is a $2F_o$–F_c electron density contoured at 1σ for verdoheme in verdoheme–HO-1. The far right figure is an overlaid comparison of the ruffled heme in heme HO-1 and flat verdoheme in verdoheme–HO-1.

The average distance in the Fe(III)–heme–HO-1 complex is 1.97 Å while that of ferrous–heme–HO-1 is 1.99 Å.

Near the α-*meso* edge, which in verdoheme is now oxygen, the wall of hydrophobic residues formed by Met34, Phe37 and Phe214 remains unchanged. On the opposite side Lys179, Arg183 and Lys18, which interact electrostatically with the propionate groups of heme in heme–HO-1, also remain unchanged in verdoheme–HO-1 even though one of the propionates is disordered. On the distal side, only the stretch of residues between Leu141 to Lys148 move closer to the verdoheme plane as noted in the previous section. Surprisingly, the distal pocket H-bonding network involving key groups generally considered important for catalysis, Asp140, Arg136 and Thr135, all remain unchanged, even though conserved waters found in all HO–heme complexes, Wat1 and Wat2, are absent in verdoheme–HO-1. It should be noted that in the ferric-biliverdin complex of rat HO-1 the residues near the α-*meso* edge, propionates and residues involved in the distal pocket H-bonding (Asp140, Arg136 and Thr135) also remain relatively unchanged from the rat heme–HO-1 structure [22]. It is clear that the essential H-bonded network in the active site is insensitive to the precise chemical nature of the prosthetic group bound in the substrate pocket.

3.4. Solvent structure of the verdoheme–HO-1 complex

Our previous structural work on human HO-1 [18,20] highlighted an important network of water molecules that is likely to be important in a proton shuttle system that participates in protonation and activation of the Fe–oxy complex. This network is consistently found in all HO structures solved to date and thus appears to be a key feature of HO catalysis [21,23,50]. In the closed molecule of heme–HO-1 the carboxylate side-chain of Asp140 forms a set H-bonds/ionic interactions with Tyr58, Arg136 and a nearby water molecule Wat1. Wat1 is in position to be a direct proton donor to the iron-linked dioxygen.

Early resonance Raman work indicated a six coordinate species for the ligand structure of the rat HO-1 ferrous–verdoheme complex, with the sixth ligand most likely being a water molecule [55]. In contrast, our structural results show that the distal water ligand, Wat0, is lost in the verdoheme complex since the iron is Fe(II) which is similar to what we found in the Fe(II)–heme complex. However, in the verdoheme structure the remaining water molecules, Wat1 and Wat2, are also missing. There is sufficient room for solvent and at very low contour levels weak density is present suggesting highly mobile waters are present but certainly not held in place by a rigid H-bonding network as in heme–HO-1. This change in solvent structure represents the most significant difference between the verdoheme complex and either the Fe(III) or Fe(II) heme complexes.

3.5. Structure of the verdoheme–NO complex

The main goal in determining the verdoheme structure in a complex with NO rather than another diatomic

ligand is to directly compare our previously published heme–NO complex structure of human HO-1 [20] with the verdoheme–NO complex. In the verdoheme–NO structure, we observe binding of NO in both the open and closed molecules compared to just the closed molecule in the heme–NO complex. Since NO bound in only the closed molecule in the heme–NO complex, we limit the following discussion on the verdoheme–NO complex to the closed molecule. Upon NO binding the distal helix moves back into a conformation similar to that found in the closed molecule of the heme–NO structure. The electron density for the NO ligand is rather diffuse and not as clearly defined as in other structures of HO complexed with NO (Fig. 6). Nevertheless, as in the heme–NO complex, the NO ligand in the verdoheme structure is bent although the bend/tilt is more pronounced. In the verdoheme complex the NO–O atom is about 3.0 Å from the α-*meso* oxygen of verdoheme, whereas in the heme–NO complex structure the distance between the oxygen atom of NO and the α-*meso* carbon of the heme is 4.0 Å.

The His–Fe bond in the verdoheme–NO structure, 2.37 Å, is rather long compared to the same bond in heme–NO, 2.12 Å. The may in part be due to the well-known ability of NO binding to loosen or even break the His–Fe bond is some heme proteins. The larger and thus weaker His–Fe bond most likely causes a weaker binding of verdoheme in verdoheme–HO-1. This may explain why verdoheme has shifted by approximately 0.5 Å away from the heme active site from the position heme normally occupies in the heme–NO structure (Fig. 7). This movement causes a change in the interactions between the one visible propionate group and protein. In the heme–NO structure the inner propionate group directly H-bonds with the side chain of Arg183 (3.03 Å), the hydroxy group of Tyr134 (2.68 Å), and through a water molecule is able to interact with the carbonyl oxygen of Ser14 and the side chain of Arg183. In verdoheme–NO this water molecule is absent and the H-bond interactions between the propionate group and residues Arg183 and Tyr134 are weaker with slightly longer distances of 3.12 and 2.98 Å, respectively. Furthermore, owing to the absence of the water molecule the propionate group no longer is able to interact with Ser14. This relatively small shifting/mobility of verdoheme in the verdoheme–NO structure may also explain the relatively diffuse electron density around the NO ligand in verdoheme–NO compared to heme–NO (Fig. 6).

The solvent structure in the heme–NO complex is organized such that the NO oxygen H-bonds with Wat1, which in turn, forms a 2.6 Å H-bond with the catalytically critical Asp140 (Fig. 6). Through Wat1 and Wat2 NO also is able to interact with the carbonyl group of Thr135. Upon binding NO in heme–HO-1, the catalytically critical Asp140 exhibits two conformations, suggesting a dynamic role for Asp140 in shuttling protons from bulk solvent via the water network to the iron-linked oxy complex. In the verdoheme–NO structure Wat1 and Wat2 are not present, and the side chain of Asp140 exhibits only one conformation, that is, the same conformation as that found in the resting state of heme–HO-1 (Fig. 6). As in the verdoheme–HO-1 structure the absence of Wat1 allows the side chain of Asp140 (OD1) to form an H-bond with the side chain (NH2) of Arg136. One final difference observed between

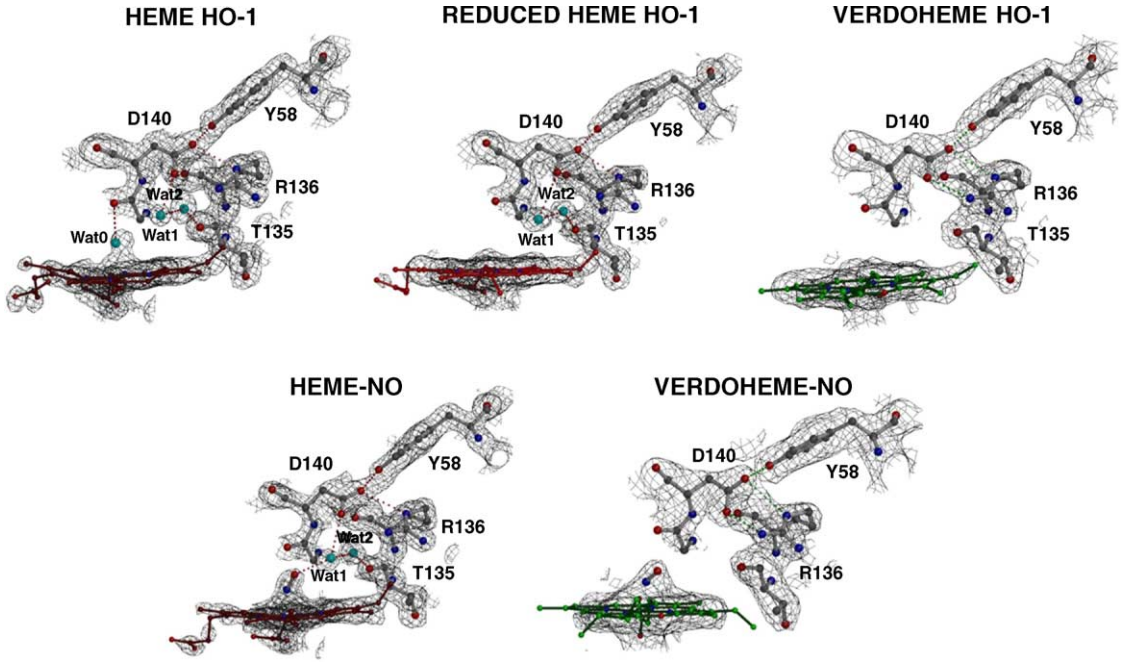

Fig. 6. $2F_o$–F_c electron density maps contoured at 1σ of the Fe(III)–heme ([12]), Fe(II)–heme ([18]), verdoheme–HO-1, and the NO complexes. The heme-bound HO-1–NO complex is taken from reference [20]. Key hydrogen bonding interactions are shown as dashed lines.

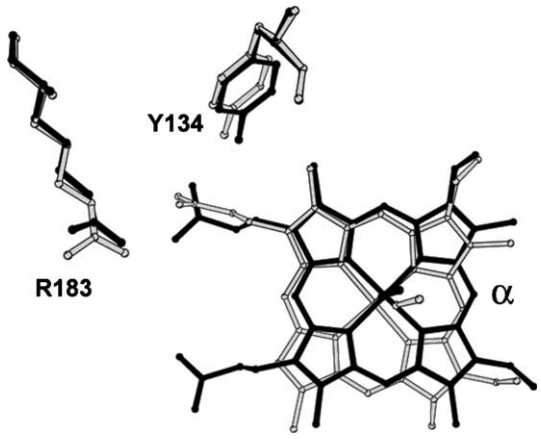

Fig. 7. Comparison of the inner propionate region between heme–NO (black) and verdoheme–NO (grey).

the NO structures is heme/verdoheme ruffling. Rivera et al. [51] pointed out that differences in heme ruffling may be part of what controls heme oxygenase chemistry. Thus, it is interesting to note that in the verdoheme–NO structure, the verdoheme is substantially flatter than the heme in heme–NO structure.

4. Discussion

The main purpose of this study was to provide further structural insights on the conversion of verdoheme to biliverdin. We focus on the verdoheme–NO complex since this is a reasonably good mimic of the catalytically relevant oxy–complex. The verdoheme appears not to be held as firmly in place as evidenced by the longer His–Fe bond, weaker density for the verdoheme substituents, and a slight displacement of the verdoheme out of the active site. Such changes are not due to steric differences since verdoheme and heme are sterically identical. However, the positive charge on the α-*meso* oxygen in verdoheme very likely creates an energetically less favorable set of interactions between the α-*meso* edge and the hydrophobic wall that forms at the back of the active site. Additionally, it is also important to consider that the reactivity of this positive charge on the α-*meso* oxygen in verdoheme is more likely susceptible to nucleophilic attack by Fe–OO^- since the reaction results in charge neutralization as opposed to electrophilic addition which has been proposed for the formation of α-*meso*-hydroxyheme [7]. This looser association of verdoheme may also contribute to the lack of ordered solvent in the active site in both the verdoheme and verdoheme–NO complexes but which are present in all heme–HO-1 complexes [20]. Nevertheless, the NO ligand tilts/bends toward the α-*meso* edge just as in the heme–NO complex although the NO ligand is bent even further toward the α-*meso* position in the verdoheme–NO complex. Such steric constraints on the orientation of the ligand ensures that the distal ox-

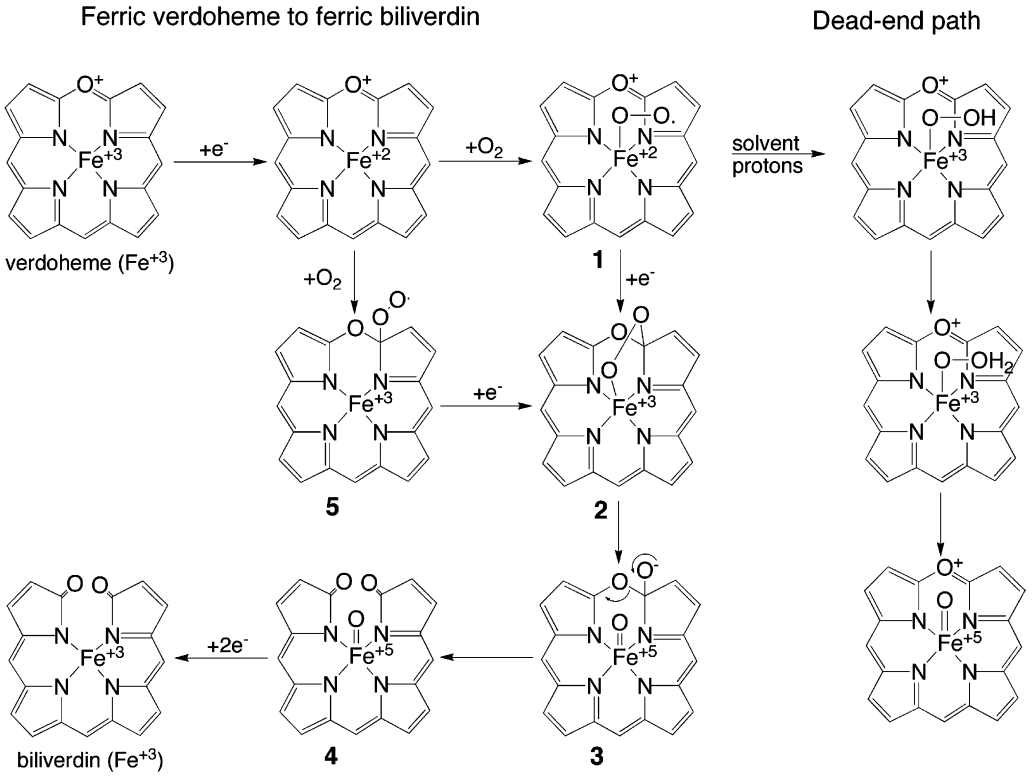

Fig. 8. Hypothetical scheme for the conversion of verdoheme to ferric biliverdin. This mechanism has been modified from its original form initially proposed by Ortiz de Montellano [41].

ygen atom (Fig. 8) reacts with correct pyrrole ring carbon. This view is supported by Zhang et al. [35] who showed using the chemically synthesized four isomers of verdoheme, that only verdoheme IXα is converted to the corresponding biliverdin IXα. This much is similar to the steric control in the initial regioselective hydroxylation of heme to give α-hydroxy *meso* heme (Fig. 1).

The most important difference in the verdoheme structures relevant to catalysis is very likely the change in active site solvent structure. The absence of ordered solvent contributes to differences in key active site groups thought to be important for proper delivery of a proton required for the initial hydroxylation of heme to α-*meso*-hydroxyheme (Fig. 1). Asp140 participates, together with Arg136 and Tyr58 and active site waters, in the proton delivery machinery required for HO-1 catalysis [20,50]. In the NO–heme complex [20], we found that Asp140 occupies two positions and may undergo an in/out motion important for catalysis. In the verdoheme–NO complex Asp140 is rigidly held in place and remains H-bonded with Arg136. This together with the fact that we do not observe Wat1 or Wat2 in the verdoheme–HO-1 structure suggests proton transfer via a rigid network of ordered solvent does not occur during the conversion of verdoheme to ferric–biliverdin which is consistent with the mechanisms previously proposed for this step [5,41,52–54]. In the traditional heterolytic fission mechanism the distal O atom is protonated by solvent protons leading to heterolytic fission of the O–O bond, water departs, and Fe(IV)–O is left. Such a process would not lead to biliverdin from verdoheme. If the oxy–verdoheme complex had access to solvent protons, then heterolytic fission of the iron-linked peroxy intermediate could occur and release water along the nonproductive pathway depicted in Fig. 8. Without competition from ordered solvent the addition of the distal O atom to the pyrrole ring carbon dominates on the productive path to biliverdin. Therefore, while the conversion of heme to α-*meso*-hydroxyheme requires both steric control and a proper proton shuttle mechanism, the conversion of verdoheme to biliverdin requires only steric control.

5. Abbreviations

HO	heme oxygenase
HO-1	mammalian HO isozyme 1
CO	carbon monoxide
Heme	Fe-protoporphyrin IX
UV	ultra violet
CNS	crystallography and NMR system

Acknowledgements

Special thanks to Profs. Angela Wilks, Alan Balch and Masao Ikeda-Saito for guidance in preparing a stable verdoheme–HO-1 complex. We thank Jayshali Lad, Jonathan Friedman, Drs. B. Bhaskar and Huying Li, during protein purification and for technical assistance during data collection at ALS. This work was supported by NIH Grants GM33688 (to T.L.P.) and DK30297 (to P.R.O.M.).

References

[1] R. Tenhunen, H.S. Marver, R. Schmid, J. Biol. Chem. 244 (1969) 6388–6394.
[2] M.D. Maines, FASEB J. 2 (1988) 2557–2568.
[3] M.D. Maines, in: Heme Oxygenase: Clinical Applications and Functions, CRC Press, Boca Raton, FL, 1992, pp. 203–266.
[4] M. Suematsu, Y. Ishimura, Hepatology 31 (2000) 3–6.
[5] P.R. Ortiz de Montellano, Curr. Opin. Chem. Biol. 4 (2000) 221–227.
[6] T. Yoshida, M. Noguchi, G. Kikuchi, J. Biol. Chem. 255 (1980) 4418–4420.
[7] R.M. Davydov, T. Yoshida, M. Ikeda-Saito, B.M. Hoffman, J. Am. Chem. Soc. 121 (1999) 10656–10657.
[8] A. Wilks, J. Torpey, P.R. Ortiz de Montellano, J. Biol. Chem. 269 (1994) 29553–29556.
[9] H. Sakamoto, Y. Omata, G. Palmer, M. Noguchi, J. Biol. Chem. 274 (1999) 18196–18200.
[10] A. Wilks, S.M. Black, W.L. Miller, P.R. Ortiz de Montellano, Biochemistry 34 (1995) 4421–4427.
[11] M. Sugishima, Y. Omata, Y. Kakuta, H. Sakamoto, M. Noguchi, K. Fukuyama, FEBS Lett. 471 (2000) 61–66.
[12] D.J. Schuller, A. Wilks, P.R. Ortiz de Montellano, T.L. Poulos, Nat. Struct. Biol. 6 (1999) 860–867.
[13] H. hou, C.T. Migita, M. Sato, D.Y. Sun, X.H. Zhang, M. Ikeda-Saito, H. Fujii, T. Yoshida, J. Am. Chem. Soc. 122 (2000) 8311–8312.
[14] Y. Liu, L.K. Lightning, H.W. Huang, P. Moenne-Loccoz, D.J. Schuller, T.L. Poulos, T.M. Loehr, P.R. Ortiz de Montellano, J. Biol. Chem. 275 (2000) 34501–34507.
[15] L.K. Lightning, H.W. Huang, P. Moënne-Loccoz, T.M. Loehr, D.J. Schuller, T.L. Poulos, P.R. Ortiz de Montellano, J. Biol. Chem. 276 (2001) 10612–10619.
[16] H. Fujii, H. Zhang, T. Tomita, M. Ikeda-Saito, T. Yoshida, J. Am. Chem. Soc. 123 (2001) 6475–6484.
[17] M. Sugishima, H. Sakamoto, Y. Kakuta, Y. Omata, S. Hayashi, M. Noguchi, K. Fukuyama, Biochemistry 41 (2002) 7293–7300.
[18] L. Lad, D.J. Schuller, J. Friedman, H. Shimizu, H. Li, P.R. Ortiz de Montellano, T.L. Poulos, J. Biol. Chem. 278 (2003) 7834–7843.
[19] M. Sugishima, H. Sakamoto, Y. Higashimoto, Y. Omata, S. Hayashi, M. Noguchi, K. Fukuyama, J. Biol. Chem. 277 (2002) 45086–45090.
[20] L. Lad, J. Wang, H. Li, J. Friedman, B. Bhaskar, P.R. Ortiz de Montellano, T.L. Poulos, J. Mol. Biol. 330 (2003) 527–538.
[21] J. Friedman, L. Lad, R. Deshmukh, H. Li, A. Wilks, T.L. Poulos, J. Biol. Chem. 278 (2003) 34654–34659.

[22] M. Sugishima, H. Sakamoto, Y. Higashimoto, M. Noguchi, K. Fukuyama, J. Biol. Chem. 278 (2003) 32352–32358.
[23] S. Hirotsu, G.C. Chu, M. Unno, D. Lee, T. Yoshida, S. Park, Y. Shiro, M. Ikeda-Saito, J. Biol. Chem. 279 (2004) 11937–11947.
[24] M. Unno, T. Matsui, G.C. Chu, M. Couture, T. Yoshida, D.L. Rousseau, J.S. Olson, M. Ikeda-Saito, J. Biol. Chem. 279 (2004) 21055–21061.
[25] L. Lad, J. Friedman, H. Li, B. Bhaskar, P.R. Ortiz de Montellano, T.L. Poulos, Biochemistry 43 (2004) 3793–3801.
[26] G. Hernandez, A. Wilks, R. Paolesse, K.M. Smith, P.R. Ortiz de Montellano, G.N. La Mar, Biochemistry 33 (1994) 6631–6641.
[27] G.N. La Mar, A. Asokan, B. Espiritu, D.C. Yeh, K. Auclair, P.R. Ortiz de Montellano, J. Biol. Chem. 276 (2001) 15676–15687.
[28] Y. Li, R.T. Syvitski, K. Auclair, A. Wilks, P.R. Ortiz de Montellano, G.N. La Mar, J. Biol. Chem. 277 (2002) 33018–33031.
[29] R.T. Syvitski, Y. Li, K. Auclair, P.R. Ortiz de Montellano, G.N. La Mar, J. Am. Chem. Soc. 124 (2002) 14296–14297.
[30] Y. Li, R.T. Syvitski, K. Auclair, P.R. Ortiz de Montellano, G.N. La Mar, J. Am. Chem. Soc. 125 (2003) 13392–13402.
[31] Y. Li, R.T. Syvitski, K. Auclair, P.R. Ortiz de Montellano, G.N. La Mar, J. Biol. Chem. 279 (2003) 10195–10205.
[32] K.M. Matera, S. Takahashi, H. Fujii, H. Zhou, K. Ishikawa, T. Yoshimura, D.L. Rousseau, T. Yoshida, M. Ikeda-Saito, J. Biol. Chem. 271 (1996) 6618–6624.
[33] Y. Liu, P.R. Ortiz de Montellano, J. Biol. Chem. 275 (2000) 5297–5307.
[34] H. Sakamoto, Y. Omata, S. Hayashi, S. Harada, G. Palmer, M. Noguchi, Eur. J. Biochem. 269 (2002) 5231–5239.
[35] X. Zhang, H. Fujii, M. Matera, C.T. Migita, D. Sun, M. Sato, M. Ikeda-Saito, T. Yoshida, Biochemistry 42 (2003) 7418–7426.
[36] A. Wilks, P.R. Ortiz de Montellano, J. Biol. Chem. 268 (1993) 22357–22362.
[37] S. Saito, H.A. Itano, Proc. Natl. Acad. Sci. USA 79 (1982) 1393–1397.
[38] T. Yoshida, M. Noguchi, J. Biochem. (Tokyo) 96 (1984) 563–570.
[39] J.C. Docherty, G.D. Firneisz, Arch. Biochem. Biophys. 235 (1984) 657–664.
[40] J.C. Docherty, B.A. Schacter, G.D. Firneisz, S.B. Brown, J. Biol. Chem. 259 (1984) 13066–13069.
[41] P.R. Ortiz de Montellano, Acc. Chem. Res. 31 (1998) 543–549.
[42] S. Saito, H.A. Itano, J. Chem. Soc. Perkin Trans 1 (1986) 1–7.
[43] D.J. Schuller, A. Wilks, P.R. Ortiz de Montellano, T.L. Poulos, Protein Sci. 7 (1998) 1836–1838.
[44] A.L. Balch, L. Latos-Grazynski, B.C. Noll, M.M. Olmstead, L. Szterenberg, N. Safri, J. Am. Chem. Soc. 115 (1993) 1422–1429.
[45] A.W.G. Leslie, Protein Crystallogr., No. 26 (1992) Joint CCP 4+ ESF-EAMCB Newsl.
[46] Z. Otwinowski, W. Minor, Methods Enzymol. 276 (1997) 307–326.
[47] A.T. Brunger, P.D. Adams, G.M. Clore, W.L. DeLano, P. Gros, R.W. Grosse-Kunstleve, J.S. Jiang, R.F. Kuszewski, M. Nilges, N.S. Pannu, R.J. Read, R.J. Rice, L.M. Rice, T. Simonson, G.L. Warren, Acta. Crystallogr. D 54 (1998) 905–921.
[48] T.A. Jones, J.Y. Zou, S.W. Cowan, M. Kieldgaard, Acta. Crystallogr. D 54 (1991) 1017–1019.
[49] R.A. Laskowski, M.W. Mac Arthur, D.S. Moss, J.M. Thornton, J. Appl. Crystallogr. 26 (1993) 283–291.
[50] M. Sugishima, H. Sakamoto, M. Noguchi, K. Fukuyama, Biochemistry 42 (2003) 9898–9905.
[51] M. Rivera, G.A. Caignan, A.V. Astashkin, A.M. Raitsimring, T.K. Shokhireva, F.A. Walker, J. Am. Chem. Soc. 124 (2002) 6077–6089.
[52] P.R. Ortiz de Montellano, A. WilksAdvances in Inorganic Chemistry, 51, Academic Press Inc., San Diego, 2001, pp. 359–407.
[53] T. Yoshida, C.T. Migita, J. Inorg. Biochem. 82 (2000) 33–41.
[54] A. Wilks, Antioxidants Redox Signal. 4 (2002) 603–614.
[55] S. Takahashi, K.M. Matera, H. Fujii, H. Zhou, K. Ishikawa, T. Yoshida, M. Ikeda-Saito, D.L. Rousseau, Biochemitsry 36 (1997) 1402–1410.